

# StereoAdapter-2: Globally Structure-Consistent Underwater Stereo Depth Estimation

Zeyu Ren<sup>1\*</sup> Xiang Li<sup>2\*</sup> Yiran Wang<sup>3\*</sup> Zeyu Zhang<sup>2\*†</sup> Hao Tang<sup>2‡</sup>

<sup>1</sup>The University of Melbourne <sup>2</sup>Peking University <sup>3</sup>Australian Centre for Robotics

\*Equal contribution. †Project lead. ‡Corresponding author: bjdxthao@gmail.com.

**Abstract**—Stereo depth estimation is fundamental to underwater robotic perception, yet suffers from severe domain shifts caused by wavelength-dependent light attenuation, scattering, and refraction. Recent approaches leverage monocular foundation models with GRU-based iterative refinement for underwater adaptation; however, the sequential gating and local convolutional kernels in GRUs necessitate multiple iterations for long-range disparity propagation, limiting performance in large-disparity and textureless underwater regions. In this paper, we propose StereoAdapter-2, which replaces the conventional ConvGRU updater with a novel ConvSS2D operator based on selective state space models. The proposed operator employs a four-directional scanning strategy that naturally aligns with epipolar geometry while capturing vertical structural consistency, enabling efficient long-range spatial propagation within a single update step at linear computational complexity. Furthermore, we construct UW-StereoDepth-80K, a large-scale synthetic underwater stereo dataset featuring diverse baselines, attenuation coefficients, and scattering parameters through a two-stage generative pipeline combining semantic-aware style transfer and geometry-consistent novel view synthesis. Combined with dynamic LoRA adaptation inherited from StereoAdapter, our framework achieves state-of-the-art zero-shot performance on underwater benchmarks with 17% improvement on TartanAir-UW and 7.2% improvement on SQUID, with real-world validation on the BlueROV2 platform demonstrates the robustness of our approach. Code: <https://github.com/AIGeeksGroup/StereoAdapter-2>. Website: <https://aigeeksgroup.github.io/StereoAdapter-2>.

## I. INTRODUCTION

Stereo depth estimation serves as a cornerstone for robotic perception, providing metric 3D reconstruction from passive binocular cameras that underpins autonomous navigation [58], manipulation, and environmental mapping. In underwater domains, accurate depth sensing is indispensable for AUV/ROV operations spanning infrastructure inspection, ecological monitoring, and archaeological survey, where geometric fidelity directly governs mission safety and autonomy [1]. Nevertheless, underwater imaging introduces pronounced domain shifts stemming from wavelength-dependent attenuation, forward and backscattering, and refraction at water–glass interfaces, which severely violate the photometric consistency assumptions underlying terrestrial stereo pipelines [42, 84].

Recent advances have sought to bridge monocular vision foundation models (VFM) [48] with stereo geometry for robust underwater adaptation. StereoAdapter [62] integrates a LoRA-adapted encoder with GRU-based iterative refinement, achieving parameter-efficient domain transfer and demonstrating promising results on underwater benchmarks. However,

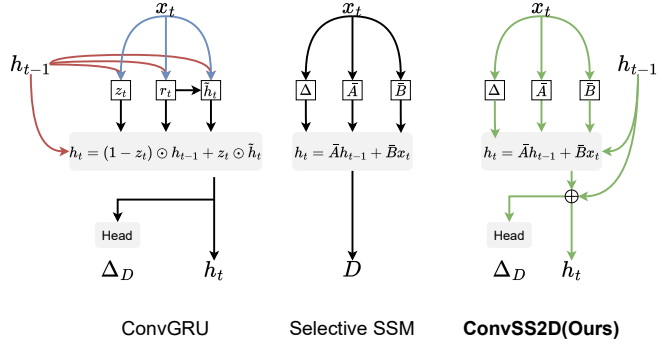


Fig. 1: Conceptual comparison. The Gated Recurrent Unit (GRU) relies on multiple non-linear gates and candidate states  $\tilde{h}_t$  to update the hidden state  $h_t$ . Its complex gating mechanism introduces non-linear recursion that is difficult to analyze for long sequences. The Selective SSM streamlines this into a linear recurrence. By dynamically generating parameters from the input  $x_t$ , the Selective SSM maintains “input-dependent selectivity” to adaptively modulate information flow. We leveraged the characteristics of selective SSM to design ConvSS2D, enabling the adaptation iterative process.

two key challenges remain for practical underwater deployment: (i) *further improving* the efficiency and accuracy of iterative disparity refinement, particularly in large-disparity and textureless regions prevalent in underwater scenes, and (ii) *bridging the synthetic-to-real gap* given the scarcity of diverse real-world underwater stereo data with accurate ground-truth annotations.

Our motivation is to advance underwater stereo depth estimation along both the architectural and data dimensions while maintaining the parameter-efficient adaptation paradigm. Concretely, we seek to explore alternative update mechanisms that can capture long-range spatial dependencies more effectively, and to construct a large-scale synthetic dataset that better covers the diversity of real underwater conditions including varying optical parameters and camera configurations.

To this end, we propose **StereoAdapter-2**, a framework that advances underwater stereo depth estimation through architectural innovation and data scaling. *Architecturally*, we introduce the ConvSS2D operator built upon selective state space models [17, 39], which employs a four-directional scanning strategy that naturally aligns with epipolar geometry while capturing vertical structural consistency, enabling

efficient long-range spatial propagation at linear computational complexity. *On the data side*, we construct **UW-StereoDepth-80K**, a large-scale synthetic underwater stereo dataset generated through a two-stage pipeline combining semantic-aware style transfer via Atlantis [78] and geometry-consistent novel view synthesis via NVS-Solver [74], systematically varying baselines, attenuation coefficients, and scattering parameters to emulate diverse ROV configurations. Combined with dynamic LoRA adaptation inherited from StereoAdapter, our framework achieves state-of-the-art zero-shot performance on underwater benchmarks, with 17% improvement on TartanAir-UW and 7.2% on SQUID, while real-world deployment on the BlueROV2 platform validates practical applicability.

The main contributions of this work are summarized as follows:

- We introduce the **ConvSS2D** update operator built upon selective state space models, replacing ConvGRU with a four-directional scanning strategy that captures both horizontal epipolar constraints and vertical structural consistency, enabling efficient long-range spatial propagation within a single refinement step.
- We construct **UW-StereoDepth-80K**, a large-scale synthetic underwater stereo dataset featuring diverse baselines and optical parameters through a two-stage generative pipeline, providing a rigorous foundation for training data-hungry stereo networks.
- We achieve state-of-the-art zero-shot performance on underwater benchmarks including TartanAir-UW and SQUID, with real-world validation on the BlueROV2 platform demonstrating robust generalization from synthetic training to real underwater scenes.

## II. RELATED WORK

*a) Deep Stereo Matching:* Early deep stereo matching methods mainly relied on CNN-based cost volume aggregation [75, 76, 50, 54, 56], where stereo correspondence is modeled by constructing and processing cost volumes using 2D or 3D convolutional architectures [2, 53, 28, 21, 73, 70, 35, 8, 79, 77, 66, 72, 51, 43, 9, 52]. However, despite these advances, CNN-based cost aggregation remains fundamentally constrained by explicit cost volume construction, motivating iterative optimization-based stereo methods that bypass explicit aggregation and enable efficient refinement on high-resolution representations [37, 34, 29, 26, 80, 53, 81, 63, 15, 10, 59, 24, 12, 65, 16, 62]. The ViT architecture transforms the stereo matching problem into a sequence-to-sequence problem [41, 55, 60, 20, 27, 40, 33, 67]. It uses self-attention and cross-attention [57] mechanisms with positional encoding to model global context and establish correspondences between stereo views, achieving competitive performance.

*b) Underwater depth estimation and datasets:* Unlike terrestrial scenarios, obtaining accurate and dense ground-truth disparity annotations in underwater environments is extremely difficult, as active sensors such as LiDAR are unreliable underwater and large-scale data collection is costly [1]. Early

underwater datasets, such as FLSea-Stereo [47], lacked accurate Stereo Disparity annotations. UWStereo proposed a high-quality synthetic underwater stereo matching dataset [42], but its scene complexity still falls short of real-world underwater scenarios.

Beyond data limitations, underwater stereo matching itself remains highly challenging. Light scattering, absorption, and refraction significantly reduce photometric consistency between views [1], making reliable matching difficult. To address these challenges, UWStereo proposed an enhancement module to better perceive geometric structures [42], while UWNet and Fast-UWNet introduced attention mechanisms and 1D-2D cross-search strategies to mitigate underwater image distortions [84]. However, these approaches rely on carefully designed, domain-specific modules for adaptation, which limits their generalization ability and scalability across diverse underwater conditions.

*c) State Space Model:* State-space model (SSM) has become an efficient alternative to Transformers in sequence modeling [38]. SSM can efficiently model long-range dependencies, and their complexity is linear or near-linear with sequence length. Unlike gated recurrent architectures, SSM relies on structured state evolution, thus achieving stable and scalable sequence processing [32, 22, 19]. Early SSM-based methods, such as S4 [18], improved computational efficiency by parameterizing the state transition matrix and reconstructing sequence modeling into convolution operations. Mamba further improved SSM by introducing selective scanning with input correlation [17, 13]. Mamba is a hardware-aware algorithm that parallelizes long sequences within a recurrent computation paradigm [17], effectively alleviating the serial bottleneck of traditional RNNs. Mamba demonstrates stronger long sequence modeling capabilities while maintaining high computational efficiency.

Following the successful application of SSM in sequence modeling, recent research has extended them to vision tasks [31, 25, 83, 39]. Vim adopts a ViT-style architecture and addresses the problem of unidirectionality and lack of positional information in SSM by introducing bidirectional processing and positional embedding [83, 14]. Vmamba further points out that visual understanding requires modeling that considers spatial structure and global relevance [39], and proposes the SS2D module, which scans images along multiple spatial directions to capture spatial dependencies. Subsequent research continues to explore improved scanning strategies and scanning direction designs to better utilize the spatial context in visual data [46, 45, 69, 23].

The scarcity of underwater scene datasets and the inherent characteristics of SS2D [39] closely match the epipolar geometry in stereo matching tasks, inspiring our approach. We leverage the rich representations learned in the pre-trained model while utilizing LoRA for efficient parameter fine-tuning and domain adaptation. Replacing the traditional GRU-based update module with an SSM-based module enables effective underwater depth estimation.

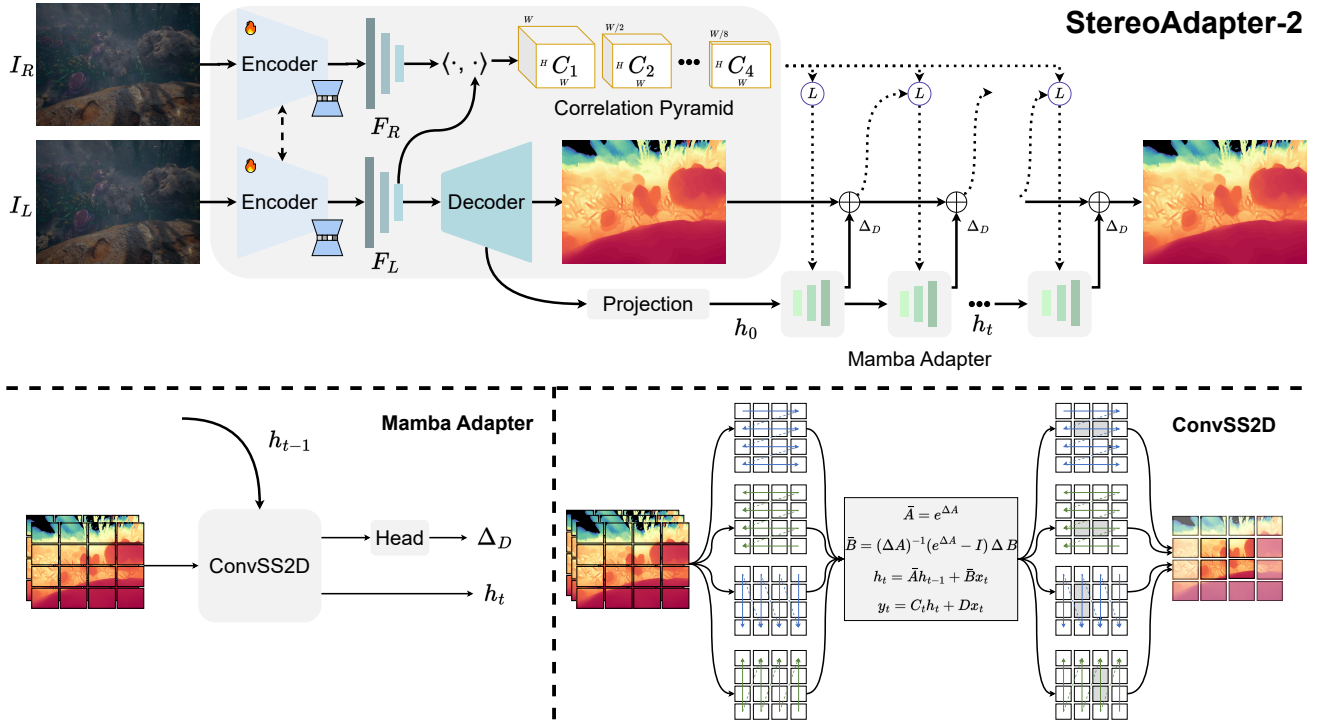


Fig. 2: Detailed architecture of the StereoAdapter-2: Our model iteratively refines disparity by integrating a Mamba Adapter. The refinement step is powered by the ConvSS2D operator, which enables adaptive and long-range spatial information propagation through multi-directional selective scanning.

### III. PRELIMINARIES

The SSM is a type of continuous-time latent state model, which defines a mapping from a one-dimensional function or sequence  $u(t) \in \mathbb{R}$  to an output  $y(t) \in \mathbb{R}$  through an implicit latent state  $h(t) \in \mathbb{R}^N$ , as given in Eq. 1.

$$\begin{aligned} h'(t) &= \mathbf{A}h(t) + \mathbf{B}u(t), \\ y(t) &= \mathbf{C}h(t) + \mathbf{D}u(t), \end{aligned} \quad (1)$$

where  $\mathbf{A}, \mathbf{B}, \mathbf{C}, \mathbf{D}$  are the learned parameters, and for the sake of explanation, we omit parameter  $D$ .

For SSM model training, we discretize the parameters of the continuous-time system. As shown in Eq. 2, the continuous-time parameters  $\mathbf{A}$  and  $\mathbf{B}$  are discretized using a zero-order hold (ZOH), where  $\Delta$  denotes the discretization time step.

$$\begin{aligned} \bar{\mathbf{A}} &= e^{\Delta \mathbf{A}}, \\ \bar{\mathbf{B}} &= (\Delta \mathbf{A})^{-1} (e^{\Delta \mathbf{A}} - \mathbf{I}) \Delta \mathbf{B}. \end{aligned} \quad (2)$$

After discretization, the entire model can be computed using linear recurrence and global convolution. Global convolution computation can be efficiently parallelized, and efficient autoregressive inference can be performed through linear recurrence.

$$\begin{aligned} \bar{\mathbf{K}} &= (\mathbf{C}\bar{\mathbf{B}}, \mathbf{C}\bar{\mathbf{A}}\bar{\mathbf{B}}, \dots, \mathbf{C}\bar{\mathbf{A}}^{L-1}\bar{\mathbf{B}}), \\ \mathbf{y} &= \mathbf{x} * \bar{\mathbf{K}}, \end{aligned} \quad (3)$$

where  $L$  is the length of the input sequence, and  $\bar{\mathbf{K}} \in \mathbb{R}^L$  denotes the structured convolutional kernel. This formulation

provides a general view of state space models, which we later reinterpret as structured spatial state recursion for iterative disparity refinement.

### IV. THE PROPOSED METHOD

#### A. Overview

We propose StereoAdapter-2, which uses a monocular depth foundation model to guide stereo disparity estimation, as shown in Fig. 2. Our framework adopts a unified architecture that integrates Depth Anything 3 [36] as both the feature encoder and monocular depth estimator. To efficiently adapt the pretrained Depth Anything 3 to stereo matching in under-water scenes, we employ LoRA [62], which enables efficient parameter fine-tuning while maintaining the rich representations learned from large-scale pre-training. Monocular depth estimation is utilized for disparity initialization to accelerate convergence. To iterate disparity estimation, we replace the traditional GRU-based update module with a Selective SSM module and enhance the learned gating mechanism. This design leverages the long-range spatial modeling capabilities of the SSM while retaining the adaptive memory control of the cyclic unit.

#### B. Feature Extraction

We first extract features  $F_L$  and  $F_R$  using the powerful depth foundation model Depth Anything 3 [36]. We extract multi-scale representations from four intermediate Transformer layers  $T^1, T^2, T^3, T^4$  to capture details and semantic

information at different levels. Meanwhile, for underwater scene domain adaptation, we fine-tune the encoder following the approach of StereoAdapter [62].

### C. Correlation Pyramids Building

We constructed a correlation pyramid to encode the visual similarity between pairs of stereo images. Unlike the optical flow of a 4D correlator that needs to cover all pixel pairs, stereo matching using calibrated images restricts the correspondences to the horizontal direction.

Given the features  $f_l^1, f_r^1 \in \mathbb{R}^{H \times W \times D}$  extracted from  $F_L$  and  $F_R$ , we compute the correlation volume by calculating the inner product between features with the same  $y$  coordinate, following Eq (4).

$$C_{ijk} = \sum_d f_{l,ijd}^1 \cdot f_{r,ikd}^1, \quad C \in \mathbb{R}^{H \times W \times W}, \quad (4)$$

where  $i$  represents the row index of the left image,  $j$  represents the column index of the left image, and  $k$  represents the column index of the right image. To capture the correspondence between fine-grained and large displacements, we construct a four-layer correlation pyramid  $C^{(l)}_{l=1}^4$  by repeatedly applying average pooling with a kernel size of 2 along the last dimension, where the  $l$ -th layer has a dimension of  $H \times W \times W/2^{l-1}$ , providing a progressively larger receptive field while maintaining spatial resolution. In each refinement iteration, given the current disparity estimate  $d$ , we perform a lookup operation using linear interpolation to retrieve the correlation values at integer offsets  $d-r, \dots, d+r$  from each pyramid layer, and concatenate the retrieved values from all layers to form the correlation features input to the update operator.

### D. Iterative Disparity Estimation

Following RAFT-Stereo [37], we adopt an iterative refinement framework to progressively estimate disparity. Given an initial disparity estimate  $D_0$ , we iteratively update it through  $L$  iterations:  $D_0, D_1, \dots, D_L$ . However, instead of using ConvGRU, We propose ConvSS2D as the core operator. Firstly, the long-range dependency modeling of ConvSS2D is achieved through sequential state recursion [17, 13, 39], without requiring multiple layers of convolutions to expand the receptive field. Specifically, the state update at spatial location  $t$  follows Eq (5).

$$h_t = \bar{A}h_{t-1} + \bar{B}x_t, \quad (5)$$

where  $h_t$  denotes the hidden state at spatial position  $t$  along a given scan direction,  $h_{t-1}$  represents the propagated state from the previous position, and  $x_t$  is the input feature at the current location. The discretized state transition matrix  $\bar{A}$  governs how information propagates sequentially across spatial positions, while  $\bar{B}$  controls how the input features are incorporated into the state update. As a result, information can be propagated over long spatial extents through directional scans, allowing features at distant locations to influence each other within a single refinement step. Owing to the inherent

long-range propagation capability of ConvSS2D, we discard the traditional context encoder and directly project decoder features to initialize the hidden state  $h_0$

*a) Input-dependent Selectivity:* A key limitation of ConvGRU lies in its inductive bias for spatial information propagation. Although its gating functions are conditioned on the input, the update is implemented through local convolutional kernels, resulting in predominantly local and isotropic information aggregation within each refinement step. In contrast, ConvSS2D introduces input-dependent selectivity through dynamically computed parameters  $\Delta$ ,  $B$ , and  $C$ . These parameters are generated from the input features  $\mathbf{x}$  via linear projections following Eq (6).

$$\Delta = \text{softplus}(W_\Delta \mathbf{x}_t), \quad B = W_B \mathbf{x}_t, \quad C = W_C \mathbf{x}_t, \quad (6)$$

where  $W_\Delta$ ,  $W_B$ ,  $W_C$  are learnable projection matrices. This mechanism enables the model to adaptively modulate: (1) the state update dynamics via  $\Delta$ , controlling the rate of state evolution; (2) input gating via  $B$ , selectively incorporating relevant features; and (3) output projection via  $C$ , emphasizing task-relevant information. Such content-aware processing allows the network to dynamically adjust its behavior based on local image characteristics, such as texture, edges, and occlusion boundaries.

*b) Scanning Strategy:* We extend one-dimensional selective scanning to two dimensions using a four-directional scanning strategy that handles features along both horizontal and vertical directions. This design is particularly suitable for stereo matching, because reliable matching still benefits from aggregating two-dimensional spatial context. The horizontal scan is directly aligned with the epipolar constraint, enabling efficient propagation of disparity information along the scan line. Simultaneously, the vertical scan contributes to consistency across the scan line, captures vertical structure, and normalizes disparity estimation in textureless regions. The outputs from all four scan directions are aggregated to form a comprehensive feature representation that satisfies the inherent geometric constraints of stereo vision.

### E. Data Synthesis: UW-StereoDepth-80K

To overcome the scarcity of diverse real-world underwater stereo data, we propose a novel two-stage generative data synthesis pipeline. Our approach leverages diffusion models to synthesize high-fidelity underwater stereo pairs from terrestrial RGB-D data. As illustrated in Fig. 3, our pipeline sequentially applies semantic-aware style transfer and geometry-consistent novel view synthesis.

*a) Underwater Style Transfer:* We utilize Atlantis [78], a specialized framework for enabling underwater data synthesis via Stable Diffusion, to bridge the photometric domain gap. Given a terrestrial source image  $I_{src}$  and its corresponding source depth map  $D_{src}$ , Atlantis acts as a style transfer module that hallucinates realistic underwater optical effects, such as wavelength-dependent attenuation, scattering, and turbidity, while preserving the semantic content and geometric structure of the original scene. By conditioning the diffusion process

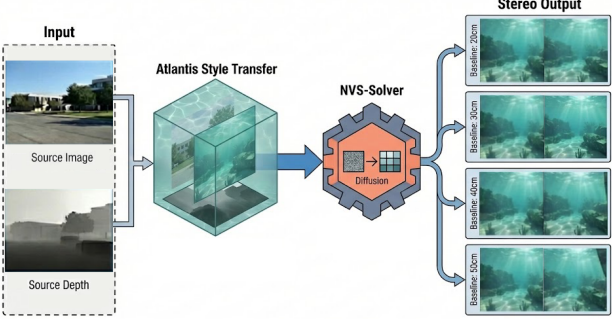


Fig. 3: Data synthesis pipeline. Semantic-aware style transfer and geometry-consistent novel view synthesis rendering pipeline for UW-StereoDepth-80K dataset.

on the source depth  $D_{src}$ , we ensure that the synthesized underwater imagery maintains structural fidelity to the input, effectively transforming a terrestrial dataset into a diverse underwater domain without losing ground truth geometric labels.

b) *Multi-Baseline Stereo Generation*: To generate stereo correspondences from the stylized monocular images, we employ NVS-Solver [74], a video diffusion model designed for zero-shot novel view synthesis. Standard diffusion-based image generation often lacks multi-view geometric consistency. NVS-Solver addresses this by treating the stereo generation task as a view synthesis problem governed by explicit camera extrinsics. Taking the output from the Atlantis stage as the reference view, we synthesize the target right view by conditioning the solver on specific baseline displacements. As shown in the right panel of Fig. 3, we systematically generate stereo pairs across four distinct baselines: 20cm, 30cm, 40cm, and 50cm. This multi-baseline strategy simulates the diverse camera configurations found in real-world underwater robots, thereby enhancing the model’s robustness to scale variations and disparity ranges during training.

c) *Dataset Construction*: By cascading Atlantis and NVS-Solver, we convert large-scale terrestrial RGB-D datasets into a synthetic underwater stereo benchmark. Each stereo pair in our generated subset is synthesized at a resolution of  $640 \times 480$ . The resulting dataset features physically plausible underwater appearance, consistent stereo geometry, and dense ground truth disparity, providing a rigorous foundation for training data-hungry stereo matching networks. UW-StereoDepth-80K is constructed by merging our newly generated diffusion-based samples with the existing UW-StereoDepth-40K dataset [62]. The final consolidated dataset comprises 80,000 high-quality stereo image pairs.

## V. EXPERIMENTS

### A. Datasets and Metrics

a) *Training Datasets*: To cover various underwater scenarios, we used our training data based on the *UW-StereoDepth-80K* dataset, which contains about 80K samples

generated using NVS-solver [74] to synthesize virtual underwater data. For evaluation, we conduct experiments on two underwater datasets. The first is *TartanAir-UW*, a subset from *TartanAir* [58] that only consists of 13,583 underwater stereo image pairs. The second is the *SQUID* dataset [6], which contains images from four distinct scenes.

b) *Evaluation Dataset and Metrics*: We report standard depth estimation metrics, including Absolute Mean Relative Error (AbsRel), Squared Mean Relative Error (SqRel), Root Mean Square Error (RMSE), and logarithmic RMSE (Log RMSE). In addition, we report accuracy under threshold metrics  $\delta_1$ ,  $\delta_2$ , and  $\delta_3$ . The accuracy threshold  $\delta_k$  measures the percentage of pixels for which  $\max\left(\frac{d_i}{\hat{d}_i}, \frac{\hat{d}_i}{d_i}\right) < 1.25^k$ , where  $d_i$  and  $\hat{d}_i$  denote the ground-truth and predicted depth values, respectively, and  $k \in \{1, 2, 3\}$ .

### B. Implementation Details

We trained StereoAdapter-2 on an H100 NVL and deployed it on ROV. Input image resolution is  $480 \times 640$  and normalized to  $[0, 1]$ . We initialize the feature encoder with Depth Anything 3 (ViT-B) [71] pretrained weights. We perform 22 iterations during training and 32 during inference. For LoRA settings, we follow the StereoAdapter [62] settings, LoRA rank  $r = 16$ , sparsity threshold  $\kappa_{\max} = 0.005$ , and regularization weight  $\lambda = 1 \times 10^{-4}$ . The sparse phase activates at 50% of training. Our method uses the loss function  $\mathcal{L}_{\text{disparity}}$  and  $\mathcal{L}_{\text{sparse}}$ , and the weight ratio is set to 1 : 1. The model is trained using the AdamW optimizer with a learning rate of  $1 \times 10^{-4}$  and weight decay of  $1 \times 10^{-5}$ . We employ the OneCycleLR scheduler for 100K iterations. Regarding data augmentation, we used strategies consistent with RAFT-Stereo [37], including saturation enhancement and random scaling.

### C. Main Results

Our experiments demonstrate that the proposed StereoAdapter-2, trained on the UW-StereoDepth-80K dataset, achieves state-of-the-art zero-shot performance across both *TartanAir* Underwater and *SQUID* benchmarks. As summarized in Tables I and II, our approach consistently outperforms existing stereo matching methods without any fine-tuning on the target domains.

As shown in Table I, StereoAdapter-2 achieves superior zero-shot performance on the *TartanAir* Underwater subset, obtaining the lowest REL (0.0440) and RMSE (2.4038), along with the highest A1 accuracy (96.76%). Compared to our prior StereoAdapter trained on UW-StereoDepth-40K, StereoAdapter-2 reduces REL by 16.5% and RMSE by 17.0%, demonstrating both the effectiveness of our adapter architecture and the benefits of scaling the training dataset.

Table II presents zero-shot evaluation on the real-world *SQUID* dataset. StereoAdapter-2 attains the best overall performance with an RMSE of 1.7481 and the lowest REL of 0.0705, reducing RMSE by 7.2% compared to the previous StereoAdapter while achieving leading accuracy across all  $\delta$  thresholds (A1: 94.25%, A2: 97.65%, A3: 98.62%). These results highlight the strong zero-shot generalization capability

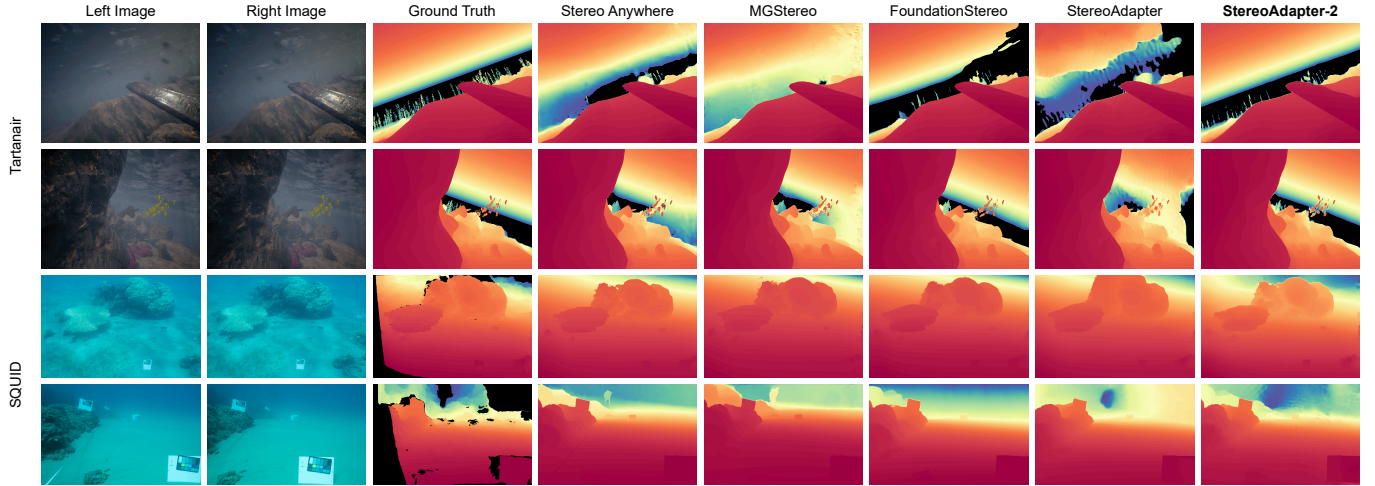


Fig. 4: Qualitative results of zero-shot stereo depth estimation

TABLE I: Quantitative comparison of zero-shot stereo depth estimation on the TartanAir underwater subset. All methods are evaluated under the same protocol using standard depth metrics.

Method	Training Set	Rel $\downarrow$	SqRel $\downarrow$	RMSE $\downarrow$	Log RMSE $\downarrow$	A1 $\uparrow$	A2 $\uparrow$	A3 $\uparrow$
LEAStereo [11]	Scene Flow	0.1099	1.3898	4.5610	0.2063	0.8929	0.9512	0.9761
PSMNet [8]	Scene Flow	0.0884	0.8699	3.9721	0.1804	0.9122	0.9627	0.9804
AANet [66]	Scene Flow	0.6096	8.3687	13.0542	0.9903	0.2598	0.3451	0.3888
GwcNet [21]	Scene Flow	0.1013	1.2965	4.1829	0.1855	0.9085	0.9612	0.9801
ACVNet [64]	Scene Flow	0.0970	1.1335	3.9985	0.1803	0.9063	0.9612	0.9813
RAFT-Stereo [37]	Scene Flow	0.0814	0.7342	4.0423	0.1703	0.9030	0.9612	0.9832
HSMNet [70]	Scene Flow	0.9856	12.3768	15.2865	4.5961	0.0000	0.0000	0.0000
TiO-Depth [82]	KITTI2012	0.7194	8.6479	13.4635	1.6967	0.0053	0.0096	0.0550
FoundationStereo [61]	FoundationStereo dataset	0.0542	0.6701	2.9644	0.1358	0.9302	0.9701	0.9779
Stereo Anywhere [4]	Scene Flow	0.0592	0.5098	3.1572	0.1544	0.9442	<b>0.9787</b>	0.9889
CREStereo [29]	ETH3D	2.5746	9.8789	8.4526	5.1297	0.4890	0.5732	0.7001
StereoAdapter [62]	UW-StereoDepth-40K	0.0527	0.5167	2.8947	0.1371	0.9467	0.9701	0.9753
<b>StereoAdapter-2 (Ours)</b>	UW-StereoDepth-80K	<b>0.0440</b>	<b>0.4312</b>	<b>2.4038</b>	<b>0.1198</b>	<b>0.9676</b>	0.9704	<b>0.9890</b>

of StereoAdapter-2 from synthetic training data to real-world underwater scenes.

As shown in Figure 4, StereoAdapter-2 generates substantially more accurate and visually coherent depth maps than baseline methods, with better scale estimation for far range details.

In summary, these findings validate that our StereoAdapter-2 architecture, combined with the UW-StereoDepth-80K dataset, enables robust zero-shot stereo depth estimation in diverse underwater environments.

#### D. Real-World Evaluation

*a) Hardware Configuration:* As shown in Figure 6, We validate our approach using a BlueROV2 platform equipped with an NVIDIA Jetson Orin NX (32GB) for onboard computation. Low-level motion control is delegated to an STM32 microcontroller. Visual input is captured by a pair of fisheye cameras mounted in a stereo arrangement; we apply offline rectification to transform the raw fisheye frames into a standard pinhole geometry prior to network inference.

*b) Scene Setup and Data Collection:* We conduct all trials in a controlled indoor water tank environment. To emulate realistic underwater navigation scenarios, we arrange glass containers and irregularly shaped stones into 5 distinct spatial layouts representing different levels of clutter complexity. The robot is then teleoperated through 3 separate navigation routes per layout, yielding a total of 15 time-aligned binocular recordings. All visual data and timestamps are logged directly on the Jetson platform.

*c) Ground-Truth Acquisition:* Before experimentation, we construct a geometrically calibrated 3D reference model of the tank interior. During each trial, camera poses are recovered by detecting AprilTags (family 16h5) and solving the corresponding pose estimation problem. These poses are subsequently aligned with the pre-scanned model, enabling us to project the geometry onto the left view and obtain per-pixel depth references. Regions without valid surface intersections are excluded from subsequent analysis.

*d) Evaluation Protocol:* Every method under comparison receives the same rectified image pairs at a uniform resolu-

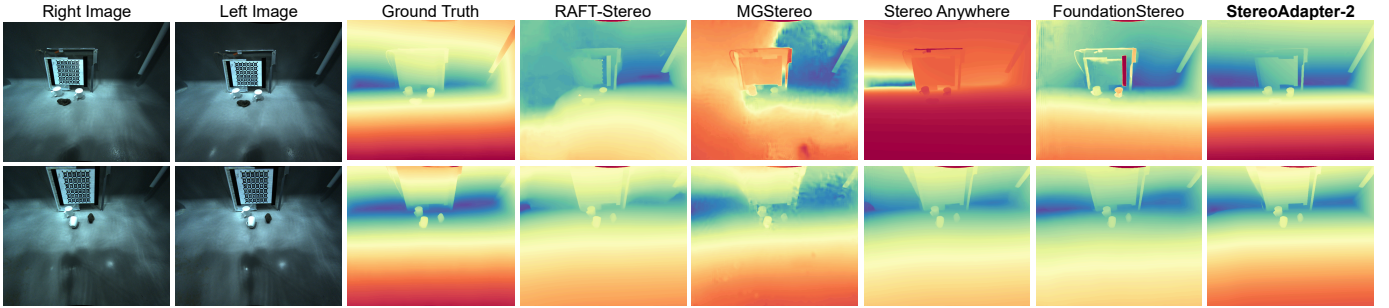


Fig. 5: Qualitative results of zero-shot underwater stereo depth estimation were obtained by deploying the model on a robotic platform.

TABLE II: Zero-shot evaluation on SQUID dataset. 5 Datasets\* refers to Scene Flow [44], Sintel [7], ETH3D [49], InStereo2K [3], and CREStereo [30].

Method	Training Set	Rel $\downarrow$	SqRel $\downarrow$	RMSE $\downarrow$	Log RMSE $\downarrow$	A1 $\uparrow$	A2 $\uparrow$	A3 $\uparrow$
LEAStereo [11]	Scene Flow	0.5574	3.9434	5.4659	0.4335	0.6512	0.8042	0.8869
PSMNet [8]	Scene Flow	0.5182	7.1404	4.9186	0.5902	0.7139	0.7999	0.8311
AANet [66]	Scene Flow	7.4801	314.1577	34.7612	1.8994	0.0602	0.1087	0.1570
GwcNet [21]	Scene Flow	0.2294	1.2275	3.0003	0.3799	0.7423	0.8517	0.9005
ACVNet [64]	Scene Flow	1.6030	65.6518	10.3828	0.7293	0.7019	0.7925	0.8321
RAFT-Stereo [37]	Scene Flow	0.0831	0.6946	1.9625	0.1441	0.9235	0.9634	0.9835
HSMNet [70]	Scene Flow	0.9772	7.2766	8.2301	4.0887	0.0000	0.0000	0.0000
CREStereo [29]	ETH3D	2.5746	9.8789	8.4526	5.1297	0.4890	0.5732	0.7001
IGEV-Stereo [63]	5 Datasets* + TartanAir	0.0932	1.4685	2.4741	0.1523	0.9346	0.9712	0.9820
Selective IGEV [59]	5 Datasets* + TartanAir	0.0960	0.9617	1.9268	0.1665	0.9171	0.9555	0.9720
GMStereo [68]	5 Datasets* + TartanAir	3.3442	140.3211	18.7829	1.0219	0.5300	0.6076	0.6578
TiO-Depth [82]	KITTI2012	1.3154	11.6828	7.0930	0.8121	0.1753	0.3346	0.5133
FoundationStereo [61]	FoundationStereo dataset	0.1095	0.7012	2.2510	0.1584	0.8995	0.9433	0.9501
Stereo Anywhere [4]	Scene Flow	0.0952	1.1017	2.4317	0.1586	0.9179	0.9605	0.9763
StereoAdapter [62]	UW-StereoDepth-40K	0.0806	0.7082	1.8843	0.1469	0.9413	0.9748	0.9852
<b>StereoAdapter-2 (Ours)</b>	UW-StereoDepth-80K	<b>0.0705</b>	<b>0.6396</b>	<b>1.7481</b>	<b>0.1285</b>	<b>0.9425</b>	<b>0.9765</b>	<b>0.9862</b>

TABLE III: Real-world evaluation on BlueROV2.

Method	REL $\downarrow$	SqRel $\downarrow$	RMSE $\downarrow$	Log RMSE $\downarrow$	A1 $\uparrow$
Stereo Anywhere [4]	0.1218	1.0623	2.4682	0.1673	0.8541
FoundationStereo [61]	0.1304	<u>0.6187</u>	2.0893	0.1635	<u>0.8812</u>
StereoAdapter [62]	0.1163	0.6794	1.9285	0.1556	0.8694
<b>StereoAdapter-2 (Ours)</b>	<b>0.1023</b>	<b>0.5843</b>	<b>1.7164</b>	<b>0.1354</b>	<b>0.9256</b>

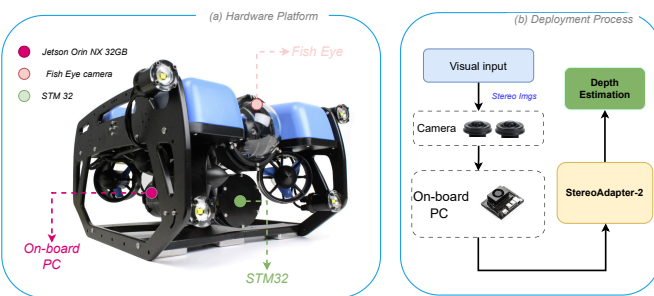


Fig. 6: Hardware platform for real world experiments.

tion with consistent pre-processing. When a model produces disparity output, we recover absolute depth via the known stereo geometry parameters. Performance is quantified using established depth metrics: Absolute Relative Error (REL), Squared Relative Error (SQ REL), Root Mean Squared Error

(RMSE), Logarithmic RMSE, and the threshold accuracy A1. All statistics are computed exclusively over valid pixels and aggregated across the full set of recordings.

*e) Results:* The proposed method achieves better performance, as shown in table III, reaching a REL of 0.1023, an RMSE of 1.7164, and A1 accuracy of 92.56%. Relative to other baselines, our proposed model exhibits consistent gains in both precision and stability across diverse underwater obstacle arrangements.

### E. Ablation Study

Table IV shows ablation experiments for different components of our model, including the use of a pre-trained model, monocular disparity initialization, ConvSS2D, and the context encoder. Table V shows the ablation experiments performed on different hyperparameter settings during model training.

Table VI further analyzes the impact of key SSM hyperparameters in ConvSS2D, including the state dimension  $d_{\text{state}}$  and the SSM expansion ratio. We observe that increasing  $d_{\text{state}}$  progressively improves model performance, with  $d_{\text{state}} = 16$  achieving the best REL and RMSE scores. However, this comes at the cost of increased computational overhead and reduced throughput. In contrast, increasing the SSM expansion

TABLE IV: Model ablation of StereoAdapter-2, evaluating the effects of different design components, including the Depth Anything 3 encoder, monocular disparity initialization, context encoder, and update module.

DA3 Encoder	Mono Disp. Init.	Context Encoder	Update Module	REL $\downarrow$	RMSE $\downarrow$
		✓	ConvGRU	0.0516	2.82
✓		✓	ConvGRU	0.0482	2.64
✓		✓	ConvSS2D	0.0449	2.46
✓			ConvSS2D	0.0463	2.54
✓	✓		ConvSS2D	<b>0.0440</b>	<b>2.40</b>

TABLE V: Ablation on training hyperparameters.

Batch Size	Learning Rate	Train Iters	REL $\downarrow$	RMSE $\downarrow$
4	$1 \times 10^{-4}$	16	0.0461	2.53
4	$2 \times 10^{-4}$	16	0.0489	2.68
8	$1 \times 10^{-4}$	16	0.0453	2.47
8	$2 \times 10^{-4}$	16	0.0476	2.59
8	$1 \times 10^{-4}$	22	<b>0.0440</b>	<b>2.40</b>

ratio beyond 1.0 leads to significant performance degradation. Considering the trade-off between accuracy and efficiency, we choose  $d_{\text{state}} = 4$  with an SSM ratio of 1.0 as the default configuration, which achieves competitive performance while maintaining high throughput. Table VII investigates the impact of different SS2D scanning modes. Compared to unidirectional and bidirectional scanning, the cross-scanning strategy consistently achieves better model performance while maintaining the number of similar parameters and FLOPs. This indicates that reliable matching still benefits from the aggregation of two-dimensional spatial context.

## VI. TEST-TIME EFFICIENCY

We evaluate on an on-board Jetson Orin NX 32GB in MaxN mode with TensorRT, batch size 1, and input resolution  $640 \times 320$ . With identical pre/post-processing for predictions. We report per-frame end-to-end latency in milliseconds (ms).

As shown in table VIII FoundationStereo and Stereo Anywhere both adopt DepthAnythingV2-L as their encoder backbone, with FoundationStereo incurring additional overhead from its transformer-based feature refinement module. MGStereo, while using a lighter encoder, involves multi-stage disparity fusion and iterative refinement, which contributes to its latency. In contrast, StereoAdapter-2 achieves the lowest latency of 1102 ms by employing a LoRA-adapted DepthAnythingV3-B encoder and replacing conventional recurrent updates with ConvSS2D, which accelerates the disparity refinement process while maintaining accuracy.

## VII. LIMITATIONS AND FUTURE WORK

Despite these advances, limitations remain. The synthetic-to-real domain gap persists under extreme underwater conditions, such as severe turbidity, strong backscatter, or rapidly varying illumination, where the diversity of our training data may not fully capture real-world complexity. Furthermore,

TABLE VI: Ablation study on ConvSS2D SSM hyperparameters under FP32 precision, analyzing the effects of the state dimension  $d_{\text{state}}$  and SSM ratio on model accuracy and efficiency.

d_state	ssm_ratio	Params (M)	FLOPs (G)	TP. (img/s)	REL $\downarrow$	RMSE $\downarrow$
1	1.0	20.40	843.33	5.26	0.0445	2.42
4	1.0	20.42	845.81	5.22	0.0440	2.40
16	1.0	20.47	855.72	4.71	<b>0.0438</b>	<b>2.38</b>
16	1.5	20.60	886.17	4.62	0.4430	2.43
16	2.0	20.73	916.62	4.26	0.4551	2.45

TABLE VII: Ablation on SS2D scanning patterns.

Scanning Pattern	Params (M)	FLOPs (G)	TP. (img/s)	REL $\downarrow$	RMSE $\downarrow$
Unidi-Scan	20.47	855.72	4.87	0.0459	2.46
Bidi-Scan	20.47	855.72	4.86	0.0453	2.42
Cross-Scan	20.47	855.72	4.74	<b>0.0440</b>	<b>2.40</b>

TABLE VIII: Average per-frame **inference latency (ms)** on Jetson Orin NX @  $640 \times 360$ , batch size=1.

Method	Params (M)	On-board (ms)
FoundationStereo [61]	375	1933
Stereo Anywhere [4]	347	1524
MGStereo [5]	347	1631
StereoAdapter [62]	202	1285
StereoAdapter-2 (Ours)	<b>103</b>	<b>1102</b>

while our method achieves strong per-frame accuracy, temporal consistency in continuous deployment remains challenging—consecutive depth predictions may exhibit flickering or instability. Future work will focus on incorporating temporal modeling to ensure prediction stability across consecutive frames, as well as exploring tighter integration with downstream robotic tasks, such as grasp point prediction for underwater manipulation.

## VIII. CONCLUSION

We present StereoAdapter-2, a novel framework for underwater stereo depth estimation by introducing the ConvSS2D operator, built upon selective state space models, our method enables efficient long-range spatial propagation through a four-directional scanning strategy. To address the scarcity of diverse underwater stereo data, we constructed UW-StereoDepth-80K through a two-stage generative pipeline, combining semantic-aware style transfer and geometry-consistent novel view synthesis, enabling systematic variation for underwater images. Combined with dynamic LoRA adaptation, our framework achieves state-of-the-art zero-shot performance on underwater benchmarks, with **17%** improvement on TartanAir-UW and **7.2%** on SQUID compared to prior methods. Real-world deployment on the BlueROV2 platform further validates the practical applicability of our approach.

## REFERENCES

[1] Derya Akkaynak and Tali Treibitz. A revised underwater image formation model. In *Proceedings of the IEEE conference on computer vision and pattern recognition*, pages 6723–6732, 2018.

[2] Antyanta Bangunharcana, Jae Won Cho, Seokju Lee, In So Kweon, Kyung-Soo Kim, and Soohyun Kim. Correlate-and-excite: Real-time stereo matching via guided cost volume excitation. In *2021 IEEE/RSJ International Conference on Intelligent Robots and Systems (IROS)*, pages 3542–3548. IEEE, 2021.

[3] Wei Bao, Wen Wang, Yuhua Xu, Yulan Guo, Siyu Hong, and Xiaohu Zhang. Instereo2k: a large real dataset for stereo matching in indoor scenes. *Science China Information Sciences*, 63, 2020. URL <https://api.semanticscholar.org/CorpusID:221110870>.

[4] Luca Bartolomei, Fabio Tosi, Matteo Poggi, and Stefano Mattoccia. Stereo anywhere: Robust zero-shot deep stereo matching even where either stereo or mono fail. In *Proceedings of the Computer Vision and Pattern Recognition Conference*, pages 1013–1027, 2025.

[5] D. Berman, T. Treibitz, and S. Avidan. Diving into haze-lines: Color restoration of underwater images. In *Proceedings of the British Machine Vision Conference*. BMVA Press, 2017.

[6] Dana Berman, Deborah Levy, Shai Avidan, and Tali Treibitz. Underwater single image color restoration using haze-lines and a new quantitative dataset. *IEEE Transactions on Pattern Analysis and Machine Intelligence*, 43(8):2822–2837, 2020.

[7] Daniel J Butler, Jonas Wulff, Garrett B Stanley, and Michael J Black. A naturalistic open source movie for optical flow evaluation. In *European Conference on Computer Vision (ECCV)*, pages 611–625, 2012.

[8] Jia-Ren Chang and Yong-Sheng Chen. Pyramid stereo matching network. In *Proceedings of the IEEE conference on computer vision and pattern recognition*, pages 5410–5418, 2018.

[9] Liyan Chen, Weihan Wang, and Philippos Mordohai. Learning the distribution of errors in stereo matching for joint disparity and uncertainty estimation. In *Proceedings of the IEEE/CVF Conference on Computer Vision and Pattern Recognition*, pages 17235–17244, 2023.

[10] Ziyang Chen, Wei Long, He Yao, Yongjun Zhang, Bingshu Wang, Yongbin Qin, and Jia Wu. Mocha-stereo: Motif channel attention network for stereo matching. In *Proceedings of the IEEE/CVF conference on computer vision and pattern recognition*, pages 27768–27777, 2024.

[11] Xuelian Cheng, Yiran Zhong, Mehrtash Harandi, Yuchao Dai, Xiaojun Chang, Hongdong Li, Tom Drummond, and Zongyuan Ge. Hierarchical neural architecture search for deep stereo matching. *Advances in Neural Information Processing Systems*, 33, 2020.

[12] Ziang Cheng, Jiayu Yang, and Hongdong Li. Stereo matching in time: 100+ fps video stereo matching for extended reality. In *Proceedings of the IEEE/CVF Winter Conference on Applications of Computer Vision (WACV)*, pages 8719–8728, January 2024.

[13] Tri Dao and Albert Gu. Transformers are SSMs: Generalized models and efficient algorithms through structured state space duality. In *International Conference on Machine Learning (ICML)*, 2024.

[14] Alexey Dosovitskiy. An image is worth 16x16 words: Transformers for image recognition at scale. *arXiv preprint arXiv:2010.11929*, 2020.

[15] Miaojie Feng, Junda Cheng, Hao Jia, Longliang Liu, Gangwei Xu, Qingyong Hu, and Xin Yang. Mc-stereo: Multi-peak lookup and cascade search range for stereo matching. *arXiv preprint arXiv:2311.02340*, 2023.

[16] Rui Gong, Weide Liu, Zaiwang Gu, Xulei Yang, and Jun Cheng. Learning intra-view and cross-view geometric knowledge for stereo matching. In *Proceedings of the IEEE/CVF conference on computer vision and pattern recognition*, pages 20752–20762, 2024.

[17] Albert Gu and Tri Dao. Mamba: Linear-time sequence modeling with selective state spaces. *arXiv preprint arXiv:2312.00752*, 2023.

[18] Albert Gu, Karan Goel, and Christopher Ré. Efficiently modeling long sequences with structured state spaces. *arXiv preprint arXiv:2111.00396*, 2021.

[19] Albert Gu, Isys Johnson, Karan Goel, Khaled Saab, Tri Dao, Atri Rudra, and Christopher Ré. Combining recurrent, convolutional, and continuous-time models with linear state space layers. *Advances in neural information processing systems*, 34:572–585, 2021.

[20] Weiyu Guo, Zhaoshuo Li, Yongkui Yang, Zheng Wang, Russell H Taylor, Mathias Unberath, Alan Yuille, and Yingwei Li. Context-enhanced stereo transformer. In *European conference on computer vision*, pages 263–279. Springer, 2022.

[21] Xiaoyang Guo, Kai Yang, Wukui Yang, Xiaogang Wang, and Hongsheng Li. Group-wise correlation stereo network. In *Proceedings of the IEEE/CVF conference on computer vision and pattern recognition*, pages 3273–3282, 2019.

[22] Ankit Gupta, Albert Gu, and Jonathan Berant. Diagonal state spaces are as effective as structured state spaces. *Advances in neural information processing systems*, 35: 22982–22994, 2022.

[23] Jie Hu, Li Shen, and Gang Sun. Squeeze-and-excitation networks. In *Proceedings of the IEEE conference on computer vision and pattern recognition*, pages 7132–7141, 2018.

[24] Yaoyu Hu, Wenshan Wang, Huai Yu, Weikun Zhen, and Sebastian Scherer. Orstereo: Occlusion-aware recurrent stereo matching for 4k-resolution images. In *2021 IEEE/RSJ International Conference on Intelligent Robots and Systems (IROS)*, pages 5671–5678. IEEE, 2021.

[25] Tao Huang, Xiaohuan Pei, Shan You, Fei Wang, Chen Qian, and Chang Xu. Localmamba: Visual state space model with windowed selective scan. *arXiv preprint*

*arXiv:2403.09338*, 2024.

[26] Junpeng Jing, Jiankun Li, Pengfei Xiong, Jiangyu Liu, Shuaicheng Liu, Yichen Guo, Xin Deng, Mai Xu, Lai Jiang, and Leonid Sigal. Uncertainty guided adaptive warping for robust and efficient stereo matching. In *Proceedings of the IEEE/CVF International Conference on Computer Vision*, pages 3318–3327, 2023.

[27] Nikita Karaev, Ignacio Rocco, Benjamin Graham, Natalia Neverova, Andrea Vedaldi, and Christian Rupprecht. Dynamicstereo: Consistent dynamic depth from stereo videos. *CVPR*, 2023.

[28] Alex Kendall, Hayk Martirosyan, Saumitro Dasgupta, Peter Henry, Ryan Kennedy, Abraham Bachrach, and Adam Bry. End-to-end learning of geometry and context for deep stereo regression. In *Proceedings of the IEEE international conference on computer vision*, pages 66–75, 2017.

[29] Jiankun Li, Peisen Wang, Pengfei Xiong, Tao Cai, Ziwei Yan, Lei Yang, Jiangyu Liu, Haoqiang Fan, and Shuaicheng Liu. Practical stereo matching via cascaded recurrent network with adaptive correlation. In *Proceedings of the IEEE/CVF conference on computer vision and pattern recognition*, pages 16263–16272, 2022.

[30] Jiankun Li, Peisen Wang, Pengfei Xiong, Tao Cai, Ziwei Yan, Lei Yang, Jiangyu Liu, Haoqiang Fan, and Shuaicheng Liu. Practical stereo matching via cascaded recurrent network with adaptive correlation. In *Proceedings of the IEEE/CVF Conference on Computer Vision and Pattern Recognition*, pages 16263–16272, 2022.

[31] Shufan Li, Harkanwar Singh, and Aditya Grover. Mamba-nd: Selective state space modeling for multi-dimensional data. In *European Conference on Computer Vision*, pages 75–92. Springer, 2024.

[32] Yuhong Li, Tianle Cai, Yi Zhang, Deming Chen, and Debadeepa Dey. What makes convolutional models great on long sequence modeling? *arXiv preprint arXiv:2210.09298*, 2022.

[33] Zhaoshuo Li, Xingtong Liu, Nathan Drenkow, Andy Ding, Francis X Creighton, Russell H Taylor, and Matthias Unberath. Revisiting stereo depth estimation from a sequence-to-sequence perspective with transformers. In *Proceedings of the IEEE/CVF international conference on computer vision*, pages 6197–6206, 2021.

[34] Zhaohuai Liang and Changhe Li. Any-stereo: Arbitrary scale disparity estimation for iterative stereo matching. In *Proceedings of the AAAI Conference on Artificial Intelligence*, volume 38, pages 3333–3341, 2024.

[35] Zhengfa Liang, Yiliu Feng, Yulan Guo, Hengzhu Liu, Wei Chen, Linbo Qiao, Li Zhou, and Jianfeng Zhang. Learning for disparity estimation through feature constancy. In *Proceedings of the IEEE conference on computer vision and pattern recognition*, pages 2811–2820, 2018.

[36] Haotong Lin, Sili Chen, Jun Hao Liew, Donny Y. Chen, Zhenyu Li, Guang Shi, Jiashi Feng, and Bingyi Kang. Depth anything 3: Recovering the visual space from any views. *arXiv preprint arXiv:2511.10647*, 2025.

[37] Lahav Lipson, Zachary Teed, and Jia Deng. Raft-stereo: Multilevel recurrent field transforms for stereo matching. In *2021 International Conference on 3D Vision (3DV)*, pages 218–227. IEEE, 2021.

[38] Xiao Liu, Chenxu Zhang, Fuxiang Huang, Shuyin Xia, Guoyin Wang, and Lei Zhang. Vision mamba: A comprehensive survey and taxonomy. *IEEE Transactions on Neural Networks and Learning Systems*, 2025.

[39] Yue Liu, Yunjie Tian, Yuzhong Zhao, Hongtian Yu, Lingxi Xie, Yaowei Wang, Qixiang Ye, Jianbin Jiao, and Yunfan Liu. Vmamba: Visual state space model. *Advances in neural information processing systems*, 37: 103031–103063, 2024.

[40] Zihua Liu, Yizhou Li, and Masatoshi Okutomi. Global occlusion-aware transformer for robust stereo matching. In *Proceedings of the IEEE/CVF Winter Conference on Applications of Computer Vision*, pages 3535–3544, 2024.

[41] Jieming Lou, Weide Liu, Zhuo Chen, Fayao Liu, and Jun Cheng. Elfnet: Evidential local-global fusion for stereo matching. *arXiv preprint arXiv:2308.00728*, 2023.

[42] Qingxuan Lv, Junyu Dong, Yuezun Li, Sheng Chen, Hui Yu, Shu Zhang, and Wenhan Wang. Uwstereo: A large synthetic dataset for underwater stereo matching. *IEEE Transactions on Circuits and Systems for Video Technology*, 2025.

[43] Yamin Mao, Zhihua Liu, Weiming Li, Yuchao Dai, Qiang Wang, Yun-Tae Kim, and Hong-Seok Lee. Uasnet: Uncertainty adaptive sampling network for deep stereo matching. In *Proceedings of the IEEE/CVF International Conference on Computer Vision*, pages 6311–6319, 2021.

[44] Nikolaus Mayer, Eddy Ilg, Philip Häusser, Philipp Fischer, Daniel Cremers, Alexey Dosovitskiy, and Thomas Brox. A large dataset to train convolutional networks for disparity, optical flow, and scene flow estimation. In *Proceedings of the IEEE Conference on Computer Vision and Pattern Recognition (CVPR)*, pages 4040–4048, 2016.

[45] Badri N Patro and Vijay S Agneeswaran. Simba: Simplified mamba-based architecture for vision and multivariate time series. *arXiv preprint arXiv:2403.15360*, 2024.

[46] Xiaohuan Pei, Tao Huang, and Chang Xu. Efficientv-mamba: Atrous selective scan for light weight visual mamba. In *Proceedings of the AAAI Conference on Artificial Intelligence*, volume 39, pages 6443–6451, 2025.

[47] Yelena Randall. Flsea: Underwater visual-inertial and stereo-vision forward-looking datasets. Master’s thesis, University of Haifa (Israel), 2023.

[48] Zeyu Ren, Zeyu Zhang, Wukai Li, Qingxiang Liu, and Hao Tang. Anydepth: Depth estimation made easy. *arXiv e-prints*, pages arXiv–2601, 2026.

[49] Thomas Schöps, Johannes L. Schönberger, Silvano Galliani, Torsten Sattler, Konrad Schindler, Marc Pollefeys, and Andreas Geiger. A multi-view stereo benchmark with high-resolution images and multi-camera videos. In

*Conference on Computer Vision and Pattern Recognition (CVPR), 2017.*

[50] Akihito Seki and Marc Pollefeys. Sgm-nets: Semi-global matching with neural networks. In *Proceedings of the IEEE conference on computer vision and pattern recognition*, pages 231–240, 2017.

[51] Zhelun Shen, Yuchao Dai, and Zhibo Rao. Cfnet: Cascade and fused cost volume for robust stereo matching. In *Proceedings of the IEEE/CVF conference on computer vision and pattern recognition*, pages 13906–13915, 2021.

[52] Zhelun Shen, Yuchao Dai, Xibin Song, Zhibo Rao, Dingfu Zhou, and Liangjun Zhang. Pcw-net: Pyramid combination and warping cost volume for stereo matching. In *European conference on computer vision*, pages 280–297. Springer, 2022.

[53] Xiao Song, Xu Zhao, Hanwen Hu, and Liangji Fang. Edgestereo: A context integrated residual pyramid network for stereo matching. In *Asian conference on computer vision*, pages 20–35. Springer, 2018.

[54] Aristotle Spyropoulos, Nikos Komodakis, and Philipppos Mordohai. Learning to detect ground control points for improving the accuracy of stereo matching. In *Proceedings of the IEEE conference on computer vision and pattern recognition*, pages 1621–1628, 2014.

[55] Qing Su and Shihao Ji. Chitransformer: Towards reliable stereo from cues. In *Proceedings of the IEEE/CVF conference on computer vision and pattern recognition*, pages 1939–1949, 2022.

[56] Fabio Tosi, Filippo Aleotti, Pierluigi Zama Ramirez, Matteo Poggi, Samuele Salti, Stefano Mattoccia, and Luigi Di Stefano. Neural disparity refinement. *IEEE Transactions on Pattern Analysis and Machine Intelligence*, 46(12):8900–8917, 2024.

[57] Ashish Vaswani, Noam Shazeer, Niki Parmar, Jakob Uszkoreit, Llion Jones, Aidan N Gomez, Łukasz Kaiser, and Illia Polosukhin. Attention is all you need. *Advances in neural information processing systems*, 30, 2017.

[58] Wenshan Wang, Delong Zhu, Xiangwei Wang, Yaoyu Hu, Yuheng Qiu, Chen Wang, Yafei Hu, Ashish Kapoor, and Sebastian Scherer. Tartanair: A dataset to push the limits of visual slam. in 2020 ieee. In *RSJ International Conference on Intelligent Robots and Systems (IROS)*, pages 4909–4916.

[59] Xianqi Wang, Gangwei Xu, Hao Jia, and Xin Yang. Selective-stereo: Adaptive frequency information selection for stereo matching. In *Proceedings of the IEEE/CVF Conference on Computer Vision and Pattern Recognition*, pages 19701–19710, 2024.

[60] Philippe Weinzaepfel, Thomas Lucas, Vincent Leroy, Yohann Cabon, Vaibhav Arora, Romain Brégier, Gabriela Csurka, Leonid Antsfeld, Boris Chidlovskii, and Jérôme Revaud. CroCo v2: Improved Cross-view Completion Pre-training for Stereo Matching and Optical Flow. In *ICCV*, 2023.

[61] Bowen Wen, Matthew Trepte, Joseph Aribido, Jan Kautz, Orazio Gallo, and Stan Birchfield. Foundationstereo: Zero-shot stereo matching. *CVPR*, 2025.

[62] Zhengri Wu, Yiran Wang, Yu Wen, Zeyu Zhang, Biao Wu, and Hao Tang. Stereoadapter: Adapting stereo depth estimation to underwater scenes. *arXiv preprint arXiv:2509.16415*, 2025.

[63] Gangwei Xu, Xianqi Wang, Xiaohuan Ding, and Xin Yang. Iterative geometry encoding volume for stereo matching. In *Proceedings of the IEEE/CVF conference on computer vision and pattern recognition*, pages 21919–21928, 2023.

[64] Gangwei Xu, Yun Wang, Junda Cheng, Jinhui Tang, and Xin Yang. Accurate and efficient stereo matching via attention concatenation volume. *IEEE Transactions on Pattern Analysis and Machine Intelligence*, 2023.

[65] Gangwei Xu, Xianqi Wang, Zhaoxing Zhang, Junda Cheng, Chunyuan Liao, and Xin Yang. Igev++: Iterative multi-range geometry encoding volumes for stereo matching. *IEEE Transactions on Pattern Analysis and Machine Intelligence*, 2025.

[66] Haofei Xu and Juyong Zhang. Aanet: Adaptive aggregation network for efficient stereo matching. In *Proceedings of the IEEE/CVF conference on computer vision and pattern recognition*, pages 1959–1968, 2020.

[67] Haofei Xu, Jing Zhang, Jianfei Cai, Hamid Rezatofighi, and Dacheng Tao. Gmflow: Learning optical flow via global matching. In *Proceedings of the IEEE/CVF conference on computer vision and pattern recognition*, pages 8121–8130, 2022.

[68] Haofei Xu, Jing Zhang, Jianfei Cai, Hamid Rezatofighi, Fisher Yu, Dacheng Tao, and Andreas Geiger. Unifying flow, stereo and depth estimation. *IEEE Transactions on Pattern Analysis and Machine Intelligence*, 45(11):13941–13958, 2023.

[69] Chenhongyi Yang, Zehui Chen, Miguel Espinosa, Linus Ericsson, Zhenyu Wang, Jiaming Liu, and Elliot J Crowley. Plainmamba: Improving non-hierarchical mamba in visual recognition. *arXiv preprint arXiv:2403.17695*, 2024.

[70] Gengshan Yang, Joshua Manela, Michael Happold, and Deva Ramanan. Hierarchical deep stereo matching on high-resolution images. In *Proceedings of the IEEE/CVF Conference on Computer Vision and Pattern Recognition*, pages 5515–5524, 2019.

[71] Lihe Yang, Bingyi Kang, Zilong Huang, Zhen Zhao, Xiaogang Xu, Jiashi Feng, and Hengshuang Zhao. Depth anything v2. *Advances in Neural Information Processing Systems*, 37:21875–21911, 2024.

[72] Menglong Yang, Fangrui Wu, and Wei Li. Wavelet-stereo: Learning wavelet coefficients of disparity map in stereo matching. In *Proceedings of the IEEE/CVF conference on computer vision and pattern recognition*, pages 12885–12894, 2020.

[73] Zhichao Yin, Trevor Darrell, and Fisher Yu. Hierarchical discrete distribution decomposition for match density estimation. In *Proceedings of the IEEE/CVF conference*

*on computer vision and pattern recognition*, pages 6044–6053, 2019.

- [74] Meng You, Zhiyu Zhu, Hui Liu, and Junhui Hou. Nvs-solver: Video diffusion model as zero-shot novel view synthesizer. *arXiv preprint arXiv:2405.15364*, 2024.
- [75] Jure Zbontar and Yann LeCun. Computing the stereo matching cost with a convolutional neural network. In *Proceedings of the IEEE conference on computer vision and pattern recognition*, pages 1592–1599, 2015.
- [76] Jure Žbontar and Yann LeCun. Stereo matching by training a convolutional neural network to compare image patches. *Journal of Machine Learning Research*, 17(65):1–32, 2016.
- [77] Jiaxi Zeng, Chengtang Yao, Lidong Yu, Yuwei Wu, and Yunde Jia. Parameterized cost volume for stereo matching. In *Proceedings of the IEEE/CVF International Conference on Computer Vision*, pages 18347–18357, 2023.
- [78] Fan Zhang, Shaodi You, Yu Li, and Ying Fu. Atlantis: Enabling underwater depth estimation with stable diffusion. In *Proceedings of the IEEE/CVF Conference on Computer Vision and Pattern Recognition*, pages 11852–11861, 2024.
- [79] Feihu Zhang, Victor Prisacariu, Ruigang Yang, and Philip HS Torr. Ga-net: Guided aggregation net for end-to-end stereo matching. In *Proceedings of the IEEE/CVF conference on computer vision and pattern recognition*, pages 185–194, 2019.
- [80] Haoliang Zhao, Huizhou Zhou, Yongjun Zhang, Yong Zhao, Yitong Yang, and Ting Ouyang. Eai-stereo: Error aware iterative network for stereo matching. In *Proceedings of the Asian conference on computer vision*, pages 315–332, 2022.
- [81] Haoliang Zhao, Huizhou Zhou, Yongjun Zhang, Jie Chen, Yitong Yang, and Yong Zhao. High-frequency stereo matching network. In *Proceedings of the IEEE/CVF conference on computer vision and pattern recognition*, pages 1327–1336, 2023.
- [82] Zhengming Zhou and Qiulei Dong. Two-in-one depth: Bridging the gap between monocular and binocular self-supervised depth estimation. *arXiv preprint arXiv:2309.00933*, 2023.
- [83] Lianghui Zhu, Bencheng Liao, Qian Zhang, Xinlong Wang, Wenyu Liu, and Xinggang Wang. Vision mamba: Efficient visual representation learning with bidirectional state space model. *arXiv preprint arXiv:2401.09417*, 2024.
- [84] Lvwei Zhu, Ying Gao, Jiankai Zhang, Yongqing Li, and Xueying Li. Reliable and effective stereo matching for underwater scenes. *Remote Sensing*, 16(23):4570, 2024.

## APPENDIX

Figure 7 shows qualitative comparisons of zero-shot stereo depth estimation on the SQUID dataset. Compared to existing methods, our approach produces more coherent disparity maps with clearer object boundaries and fewer artifacts in textureless and low-contrast underwater regions. Figure 8 shows qualitative results obtained on a real-world robotic platform. The proposed method demonstrates stable and consistent depth predictions under real underwater conditions.

Figure 9 shows qualitative zero-shot stereo depth estimation results on the TartanAir Ocean dataset. Our method preserves fine-grained structural details and large-disparity regions more effectively, indicating strong generalization under diverse underwater appearances. Figure 10 shows representative samples from the proposed UW-StereoDepth-80K dataset. The dataset covers diverse underwater scenes, baselines, providing rich supervision for large-scale underwater stereo adaptation.

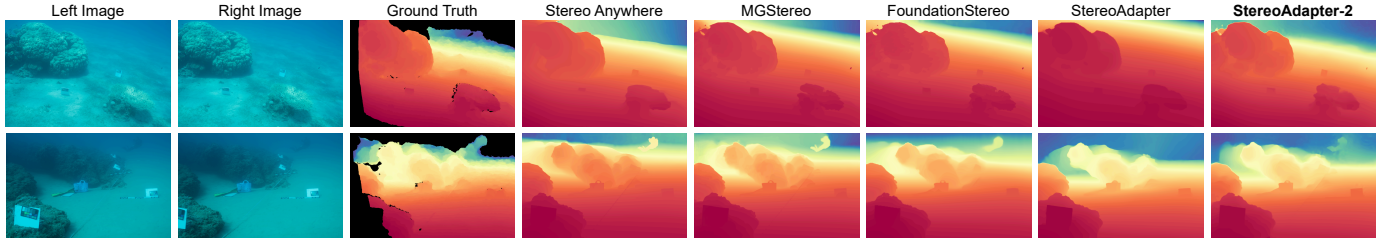


Fig. 7: Qualitative results of zero-shot stereo depth estimation for different models on the SQUID dataset.

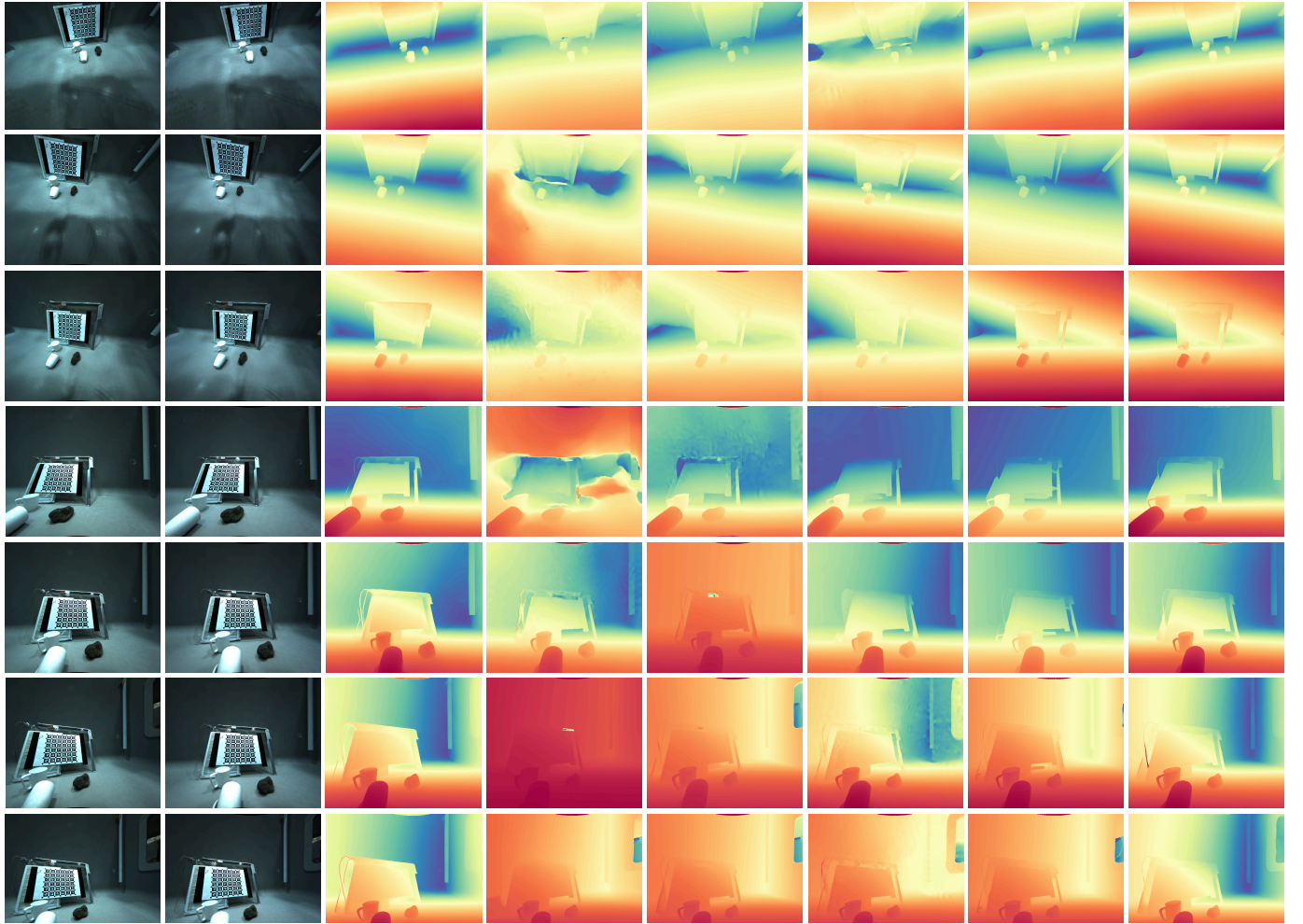


Fig. 8: Qualitative results of zero-shot stereo depth estimation for different models on the robot platform.

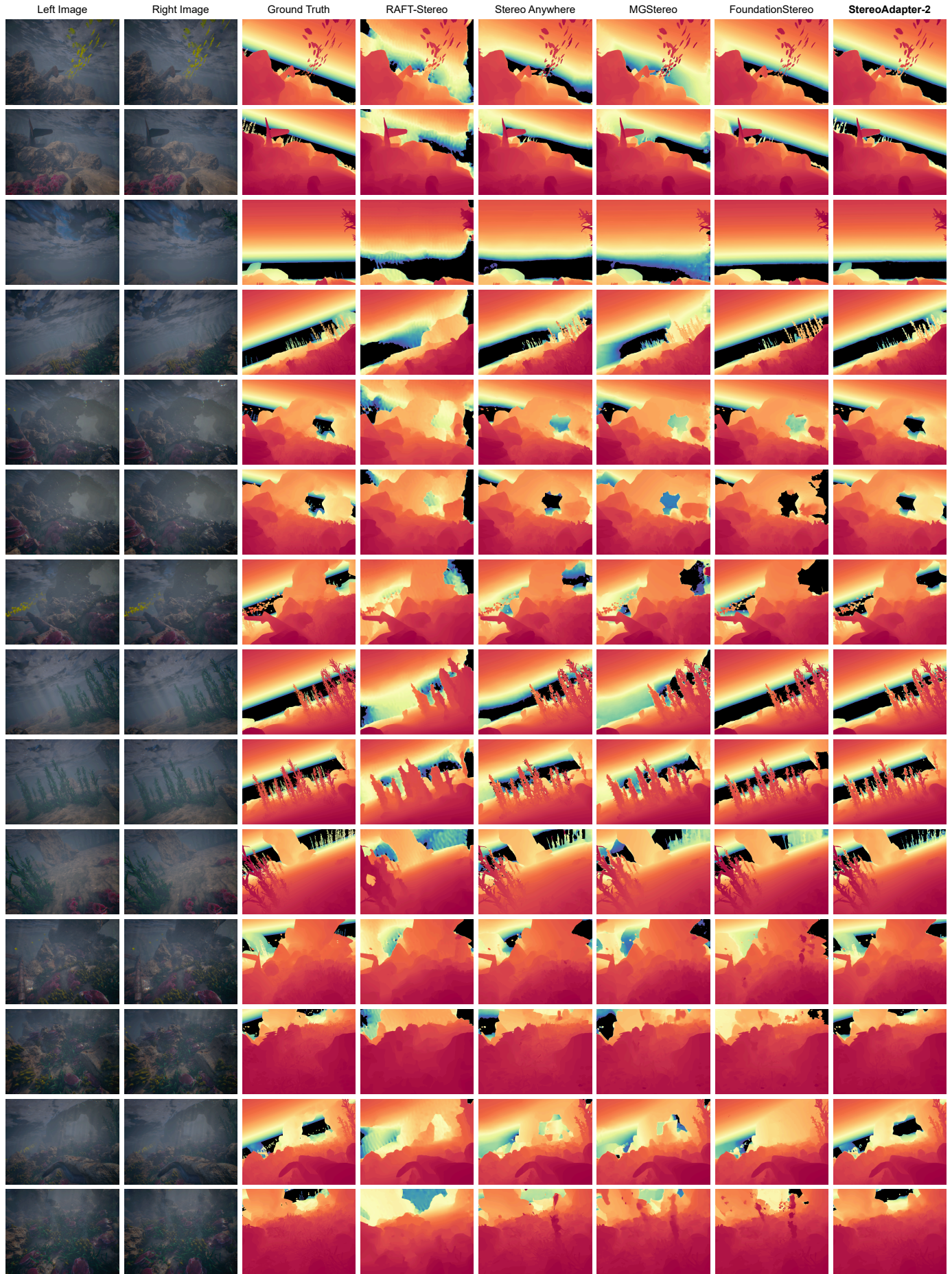


Fig. 9: Qualitative results of zero-shot stereo depth estimation for different models on the Tartanair Ocean dataset

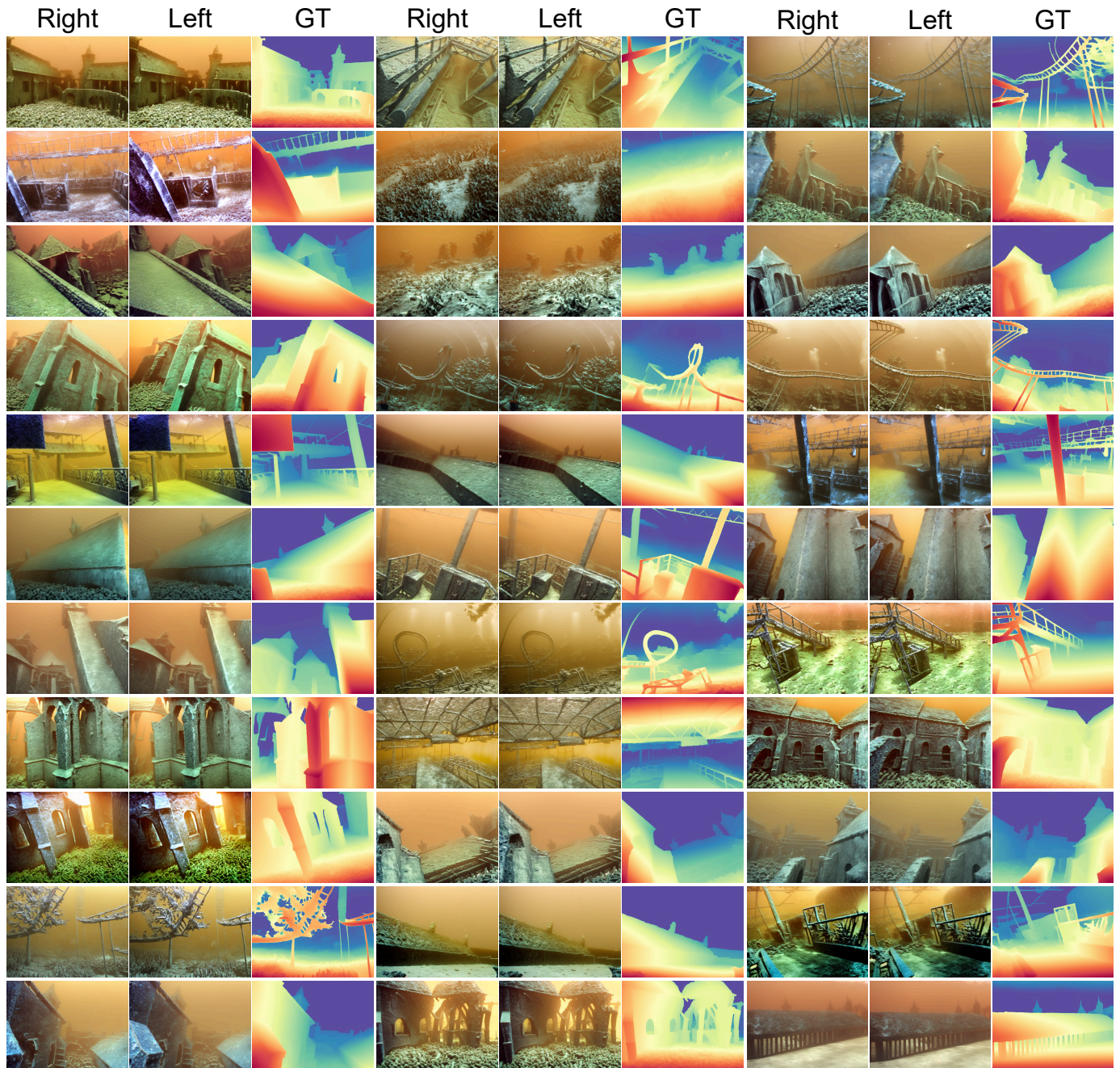


Fig. 10: Visualization of UW-StereoDepth-80K